

Electroweak phase transition and gravitational waves in a two-component dark matter model

Ahmad Mohamadnejad^{*1}

¹Department of Physics, Lorestan University, Khorramabad, Iran

April 4, 2022

Abstract

We investigate an extension of the Standard Model (SM) with two candidates for dark matter (DM). One of them is a real scalar field and the other is an Abelian gauge field. Except for these two, there is another beyond SM field which has unit charge under a dark $U_D(1)$ gauge symmetry. The model is classically scale invariant and the electroweak symmetry breaks because of the loop effects. Although SM is extended with a new dark symmetry and three fields, because of scale invariance, the parameter space is strictly restricted compared to other two-component DM models. We study both DM phenomenology and electroweak phase transition and show that there are some points in the parameter space of the model consistent with DM relic density and direct detection constraints, while at the same time can lead to first order electroweak phase transition. The gravitational waves produced during the phase transition could be probed by future space-based interferometers such as Laser Interferometer Space Antenna (LISA) and Big Bang Observer (BBO).

^{*}mohamadnejad.a@lu.ac.ir

Contents

1	Introduction	2
2	The model	4
3	Dark matter phenomenology	5
3.1	Relic density	5
3.2	Direct detection	7
4	Electroweak phase transition	10
4.1	One-loop effective potential	10
4.2	First order phase transition and gravitational waves	13
5	Results	17
6	Conclusion	21

1 Introduction

The standard model (SM) is the most successful model in describing the observed phenomena, however, there are still intriguing questions, such as the nature and the origin of dark matter (DM), waiting to be answered. There is a wide variety of astrophysical and cosmological observations as well as theoretical arguments that led the scientific community to adopt DM as an essential part of the standard cosmological model (for a fascinating review on history of DM see [1]).

The evidence of DM was strong enough that many strategies have been pursued to reveal its particle nature. For decades, the leading theory of particle DM was a single-component thermal relic with weak size couplings and mass, known as a weakly interacting massive particle (WIMP). These one-component scenarios are increasingly constrained by experimental measurements. Therefore, workers in the field compelled to examine more complex models of dark sector including the multicomponent ones where the total relic abundance of DM is due to the existence of multiple DM species [2–45]. After all, it should not be surprising if the dark sector has multiple species like SM itself.

On the other hand, SM has a crossover rather than a true phase transition [46], while some extensions of the SM, e.g., with DM candidates [47–72], lead to first order phase transitions with gravitational wave (GW) signals. In the case of first order phase transition, just below the critical temperature, the Universe goes from a metastable quasi-equilibrium state into a stable equilibrium state, through a process of bubble nucleation, growth, and merger which generates GWs [73–77]. GW signatures are therefore a new window towards new physics, complementary to that provided by the Large Hadron Collider. Another motivation for studying electroweak phase transitions is the requirements to explain the matter-antimatter asymmetry in the universe [78], which one of them, departure from thermal equilibrium, is inevitable in a first-order phase transition.

The first direct detection of GWs was performed in 2015 [79]. The signal came from the strongest astrophysical sources of GWs, i.e., compact binary systems, in frequency from 35 to 250 Hz. Here, we are interested in production of GWs by first-order phase transitions (for a recent review see [80]). For GWs sourced by cosmological phase transitions, the relevant mission is Laser Interferometer Space Antenna (LISA) [81] which is a space-based interferometric gravitational wave detector working with three satellites orbiting the Earth. LISA is most sensitive at frequencies in the range $10^{-3} - 10^{-2}$ Hz and its planned launch year is 2034 with a mission life-time of 4 years. The Big Bang Observer (BBO) [82] is a proposed follow-up experiment consisting of four LISA-like detectors.

In this paper, a model with three motives will be presented. We come up with a beyond SM model to provide a solution for DM problem, hierarchy problem, and vacuum instability. As a solution for hierarchy problem [83], the model has classical conformal symmetry. On the other hand, SM suffers from vacuum instability and beyond SM models with bosonic degrees of freedom can probably solve this issue. As mentioned, due to the strict constraints of direct detection on one-component DM models, two component DM models are more appropriate. Therefore, our two-component DM model consists (bosonic) scalar and vector DM. We assume that the dark sector interacts with the SM particles only through the Higgs portal. The dark sector consists of three new fields, a real scalar, a complex singlet and a real vector field and it introduces a dark $U_D(1)$ gauge symmetry. Our model is a two-component DM model which both DM particles are bosons: one DM particle is spin zero and the other is spin one. As a potential solution to the hierarchy problem, we constrain our model to be a classically scale-invariant extension of the SM. Within this framework, all the particle masses are generated dynamically, by means of the Coleman-Weinberg mechanism [84]. After constructing the model, we study DM phenomenology including relic density and DM-Nucleon cross section. DM relic density is reported by Planck Collaboration [85], and DM-Nucleon cross section is constrained by direct detection experiments such as the LUX [86], PandaX-II [87] and XENON1T [88]. These experiments are gradually approaching the so-called neutrino floor which is the ultimate sensitivity of future direct detection experiments [89]. We also concentrate on investigating the possibility of achieving a strongly first-order electroweak phase transition within the parameter space of the model. To study electroweak phase transition, we present the complete expression of the finite-temperature 1-loop effective potential, including the contributions of the resummed thermal bosonic daisy diagrams, and show that the finite-temperature corrections induce a first-order electroweak phase transition. We identify regions of parameter space of the model which is consistent with DM relic density and direct detection constraints, while simultaneously realizing a strongly first-order electroweak phase transition. The GW signal from the phase transition is sufficiently strong to be detectable by LISA and BBO.

The rest of the paper is organized as follows. In section 2, we introduce our model. Section 3 is dedicated to DM phenomenological constraints. In section 4, we study the electroweak phase transition and GWs spectrum. Our result is given in section 5 where we simultaneously consider DM phenomenology and GW spectrum using two benchmark points (BMs) as shown in table 1. Finally, we conclude in section 6.

2 The model

Our model consists three beyond SM fields which all of them are bosons, namely, a complex singlet ϕ , a real singlet S , and a real Abelian vector field V_μ . In our setup, the complex scalar field ϕ has unit charge under a dark $U_D(1)$ gauge symmetry with the vector field V_μ . All of these fields are singlet under SM gauge group. However, the dark sector is invariant under the charge conjugation of $U_D(1)$ and parity of S :

$$\phi \rightarrow \phi^*, \quad V_\mu \rightarrow -V_\mu, \quad \text{and} \quad S \rightarrow -S. \quad (2.1)$$

Due these two symmetries, the model can have two component DM. In the dark sector the discrete symmetry $V_\mu \rightarrow -V_\mu$ forbids the kinetic mixing between the SM $U_Y(1)$ gauge boson B_μ and the vector field V_μ which makes V_μ stable and a DM candidate. The other DM candidate is due to $S \rightarrow -S$ symmetry which makes the real singlet field stable.

The Lagrangian is given by

$$\mathcal{L} = \mathcal{L}_{\text{SM}} + \frac{1}{2}(\partial_\mu S)(\partial^\mu S) + (D_\mu \phi)^*(D^\mu \phi) - \frac{1}{4}V_{\mu\nu}V^{\mu\nu} - V(H, \phi, S), \quad (2.2)$$

where $V_{\mu\nu} = \partial_\mu V_\nu - \partial_\nu V_\mu$, $D_\mu \phi = (\partial_\mu + igV_\mu)\phi$, and \mathcal{L}_{SM} is the SM Lagrangian without the Higgs potential term.

We constrain $V(H, \phi, S)$ by:

- gauge symmetry,
- Z_2 symmetry,
- scale invariance, and
- renormalizability.

Regarding these constraints $V(H, \phi, S)$ reads

$$V(H, \phi, S) = \lambda_H(H^\dagger H)^2 + \lambda_\phi(\phi^* \phi)^2 + \lambda_{H\phi}(H^\dagger H)(\phi^* \phi) + \frac{1}{2}\lambda_{HS}(H^\dagger H)S^2 + \frac{1}{2}\lambda_{\phi S}(\phi^* \phi)S^2 + \frac{1}{4}\lambda_S S^4. \quad (2.3)$$

In this model, dark sector interacts with SM via Higgs portal. Because of Z_2 symmetry, the real singlet field, S , does not get vacuum expectation value (VEV), but electroweak symmetry, as well as Abelian dark symmetry spontaneously break after H and ϕ develop VEVs. In the unitary gauge, $H^\dagger = (0, \frac{h_1}{\sqrt{2}})$ and $\phi = \frac{h_2}{\sqrt{2}}$, the tree level potential is given by

$$V_{\text{tree}}(h_1, h_2, S) = \frac{1}{4}\lambda_H h_1^4 + \frac{1}{4}\lambda_\phi h_2^4 + \frac{1}{4}\lambda_{H\phi} h_1^2 h_2^2 + \frac{1}{4}\lambda_{HS} h_1^2 S^2 + \frac{1}{4}\lambda_{\phi S} h_2^2 S^2 + \frac{1}{4}\lambda_S S^4. \quad (2.4)$$

The local minimum of the tree level potential defines the VEVs of the fields which we take as $(\langle h_1 \rangle, \langle h_2 \rangle, \langle S \rangle) = (\nu_1, \nu_2, 0)$, leading to the following condition

$$\lambda_H > 0 \wedge \lambda_{H\phi} < 0 \wedge \lambda_\phi = \frac{\lambda_{H\phi}^2}{4\lambda_H} \wedge \frac{\nu_1}{\nu_2} = \sqrt{-\frac{\lambda_{H\phi}}{2\lambda_H}}. \quad (2.5)$$

The last relation defines the flat direction in field space where the tree level potential is minimum, along this direction $V_{tree}(\nu_1, \nu_2, 0) = 0$. Now we substitute $h_1 \rightarrow \nu_1 + h_1$ and $h_2 \rightarrow \nu_2 + h_2$ which mixes h_1 and h_2 . The mass eigenstates, h and φ , can be obtained from the following rotation

$$\begin{pmatrix} h \\ \varphi \end{pmatrix} = \begin{pmatrix} \cos\alpha & -\sin\alpha \\ \sin\alpha & \cos\alpha \end{pmatrix} \begin{pmatrix} h_1 \\ h_2 \end{pmatrix}, \quad (2.6)$$

where $\tan\alpha = \nu_1/\nu_2$ ($\langle h \rangle = 0$ and $\langle \varphi \rangle = \nu = \sqrt{\nu_1^2 + \nu_2^2}$). We identify h , which is perpendicular to the flat direction, as the SM-like Higgs observed at the LHC with $M_h = 125$ GeV [91, 92]. On the other hand, we know from SM that $\nu_1 = 246$ GeV. The field φ is along the flat direction, thus its tree level mass is zero. However, 1-loop correction leads to a specific value along flat direction as the minimum of the potential which gives the following mass to φ (see subsection 4.1):

$$M_\varphi^2 = \frac{1}{8\pi^2\nu^2} (M_h^4 + M_S^4 + 3M_V^4 + 6M_W^4 + 3M_Z^4 - 12M_t^4), \quad (2.7)$$

where $M_{S,V,W,Z,t}$ being the masses for scalar DM, vector DM, W and Z gauge bosons, and top quark, respectively, after symmetry breaking. We can substitute the parameters of the Lagrangian using

$$\begin{aligned} \lambda_{H\phi} &= -\frac{M_h^2}{\nu^2}, \lambda_\phi = \frac{M_h^2}{2\nu^2} \tan^2\alpha, \lambda_H = \frac{M_h^2}{2\nu^2} \cot^2\alpha, \\ M_V &= g \cos\alpha \nu, M_S^2 = \frac{1}{2} (\lambda_{\phi S} \cos^2\alpha + \lambda_{HS} \sin^2\alpha) \nu^2. \end{aligned} \quad (2.8)$$

According to these relations there are five free parameters which we choose them as $M_S, M_V, g, \lambda_{\phi S}$, and λ_S . On the other hand, λ_S is irrelevant in DM phenomenology and phase transition studied in this paper, therefore we left with only four parameters.

3 Dark matter phenomenology

In the following we will focus on the DM relic density constraint reported by Planck collaboration [85] and the available data on direct DM detection.

3.1 Relic density

It is considered in general that in WIMP scenarios, the DM relic density is inversely proportional to the thermally averaged DM annihilation cross section into SM particles. In the case of two-component DM, the situation is more interesting since there are additional important processes such as conversion of one DM component into another which complicates the analysis. We use the public numerical code `micrOMEGAs` [93] for solving the two Boltzmann equations governing the cosmological evolution of our DM candidates, the scalar DM (S) and the Vector DM (V). The Boltzmann equations are determined by three types of processes:

- DM Annihilation: pair annihilation of both DM components into SM particles,
- DM Conversion: which converts one DM component into another, and

- DM Semi-(co)annihilation: which could change the abundances of both DM components

The relevant diagrams for the annihilation processes of the two DM components are presented in figure 1. There are no (subleading) semi-annihilation and co-annihilation processes in our scenario. As we see in figure 1, Feynman diagrams are the same for both DM components. In these figure, SM and \overline{SM} stand for massive SM particles and anti-particles, respectively. Besides DM annihilation into SM particles, the two DM candidate can also annihilate into each other (DM conversion: $S S \longleftrightarrow V V$) which are shown in figure 2.

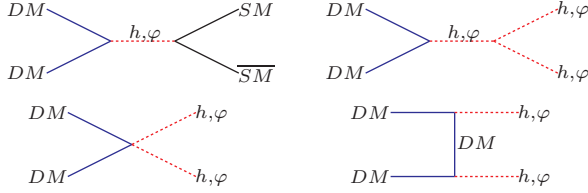


Figure 1: Pair annihilation processes for both scalar and vectorial DM components.

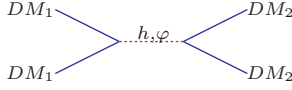


Figure 2: DM conversion via Higgs portal.

The coupled Boltzmann equations for scalar S and vector V DM are given by:

$$\frac{dn_V}{dt} + 3Hn_V = - \sum_j \langle \sigma_{VV \rightarrow jj} v \rangle (n_V^2 - n_{V,eq}^2) - \langle \sigma_{VV \rightarrow SS} v \rangle (n_V^2 - n_{V,eq}^2 \frac{n_S^2}{n_{S,eq}^2}), \quad (3.1)$$

$$\frac{dn_S}{dt} + 3Hn_S = - \sum_j \langle \sigma_{SS \rightarrow jj} v \rangle (n_S^2 - n_{S,eq}^2) - \langle \sigma_{SS \rightarrow VV} v \rangle (n_S^2 - n_{S,eq}^2 \frac{n_V^2}{n_{V,eq}^2}), \quad (3.2)$$

where j runs over SM massive particles and h, φ . By changing the variable, $x = M/T$ and $Y = n/s$, where T is the photon temperature and s is the entropy density, one can rewrite the Boltzmann equations in terms of $Y = n/s$:

$$\begin{aligned} \frac{dY_V}{dx} = & - \sqrt{\frac{45}{\pi}} M_{pl} g_*^{1/2} \frac{M}{x^2} [\sum_j \langle \sigma_{VV \rightarrow jj} v \rangle (Y_V^2 - Y_{V,eq}^2) \\ & + \langle \sigma_{VV \rightarrow SS} v \rangle (Y_V^2 - Y_{V,eq}^2 \frac{Y_S^2}{Y_{S,eq}^2})], \end{aligned} \quad (3.3)$$

$$\begin{aligned} \frac{dY_S}{dx} = & -\sqrt{\frac{45}{\pi}} M_{pl} g_*^{1/2} \frac{M}{x^2} \left[\sum_j \langle \sigma_{SS \rightarrow jjv} \rangle (Y_S^2 - Y_{S,eq}^2) \right. \\ & \left. + \langle \sigma_{SS \rightarrow VVv} \rangle (Y_S^2 - Y_{S,eq}^2 \frac{Y_V^2}{Y_{V,eq}^2}) \right], \end{aligned} \quad (3.4)$$

where $g_*^{1/2}$ is the degrees of freedom parameter and M_{pl} is the Planck mass. The last terms in summations are new terms in Boltzmann equations which describe the conversion of DM particles into each other. Since these two cross sections are described by the same matrix element, we expect $\langle \sigma_{VV \rightarrow SSv} \rangle$ and $\langle \sigma_{SS \rightarrow VVv} \rangle$ are not independent and their relation is:

$$Y_{V,eq}^2 \langle \sigma_{VV \rightarrow SSv} \rangle = Y_{S,eq}^2 \langle \sigma_{SS \rightarrow VVv} \rangle. \quad (3.5)$$

The interactions between the two DM candidates take place by exchanging two scalar mass eigenstates h and φ where the coupling of V to h is suppressed by $\sin \alpha$. Therefore, it is usually the φ -mediated diagram that gives the dominant contribution. Notice that the conversion of the heavier particle into the lighter one is relevant. The relic density for each DM candidate is related to Y at the present temperature through $\Omega_{S,V} h^2 = 2.755 \times 10^8 \frac{M_{S,V}}{GeV} Y_{S,V}(T_0)$, where h is the Hubble expansion rate at present times in units of 100 $(km/s)/Mpc$, and the total relic density of DM according to the data by the Planck collaboration should be [85],

$$\Omega_{DM} h^2 = \Omega_S h^2 + \Omega_V h^2 = 0.120 \pm 0.001. \quad (3.6)$$

Finally, we define the fraction of the DM density of each component by,

$$\xi_V = \frac{\Omega_V}{\Omega_{DM}}, \quad \xi_S = \frac{\Omega_S}{\Omega_{DM}}, \quad \text{with } \xi_V + \xi_S = 1. \quad (3.7)$$

Figure 3 depicts the relic density of both DM components as a function of free parameters of the model. According to these figure, $\lambda_{\phi S}$, and M_S are not relevant in Ω_V (Note that, in general, Ω_V depends on M_S , because M_φ is a function of M_S). However, Ω_S depends on all four parameters. In this case, besides $\lambda_{\phi S}$ and M_S which are relevant, λ_{HS} can also change Ω_S . On the other hand, considering eq. (2.8), λ_{HS} is dependent in all free parameters:

$$\lambda_{HS} = \frac{2M_S^2/\nu^2 - \lambda_{\phi S} \cos^2 \alpha}{\sin^2 \alpha} = \frac{1}{\nu_1^2} \left(2M_S^2 - \frac{\lambda_{\phi S}}{g^2} M_V^2 \right). \quad (3.8)$$

So it is not a surprise that all free parameters can effect the relic density of scalar DM. The minimum in figure 3 (c) at $M_S \simeq \frac{M_h}{2}$ is due to resonance, and maximum in all four diagrams is due to $\lambda_{HS} \simeq 0$.

3.2 Direct detection

The direct detection experiments aim to study DM-Nucleon interactions. These events induced by DM particles from the Milky Way's halo. The Standard Halo Model assumes that the DM particles are distributed in an isotropic isothermal sphere with a Maxwellian velocity distribution. The local DM density ρ_0 adopted for the interpretation of direct detection experiments is $\rho_0 = 0.3 GeV/c^2/cm^3$. The possibility of DM direct detection

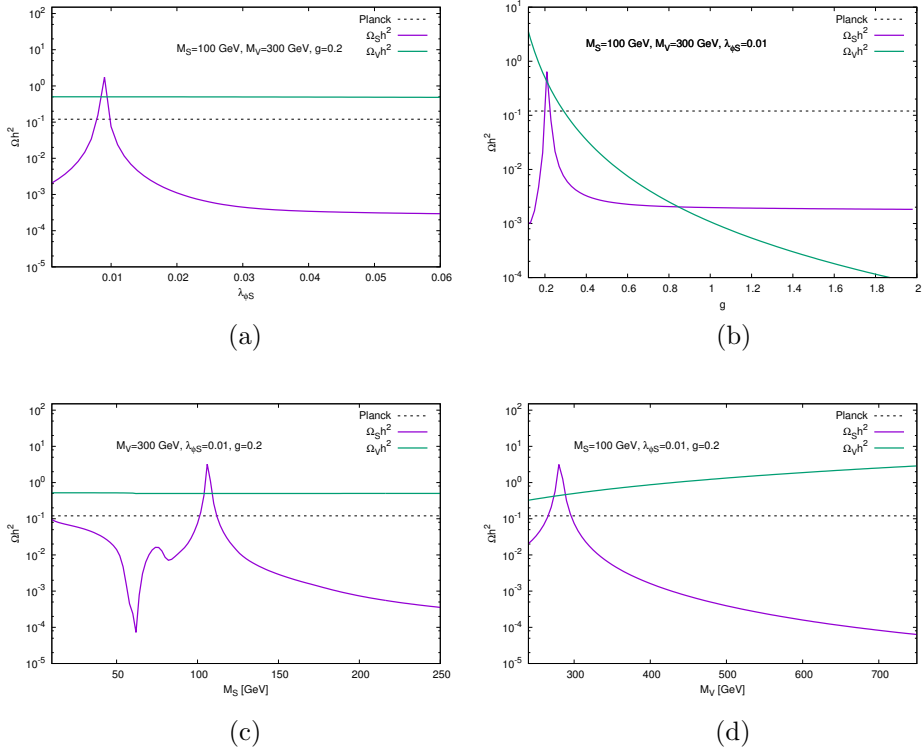


Figure 3: Variation of DM Relic density respect to parameter space

in the form of WIMPs was first discussed in [94]. The idea is simple: since in most scenarios the WIMP carries no electric charge, therefore it will not interact with the atomic electrons, however, DM particles can elastically scatter off the atomic nucleus and the momentum transfer gives rise to a nuclear recoil which might be detectable.

In our model both DM candidates interact with quarks via Higgs portal, see figure 4, which results in a spin independent DM-Nucleon cross section.

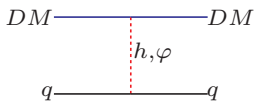


Figure 4: DM-quark interaction via t channel exchanges of the h and φ states.

The relevant DM-quark interaction terms in Lagrangian are:

$$\begin{aligned}
\mathcal{L}_q &= -\sum_q \frac{m_q}{\nu_1} \cos \alpha h \bar{q}q + \frac{m_q}{\nu_1} \sin \alpha \phi \bar{q}q, \\
\mathcal{L}_S &= \lambda_{hss} h S^2 + \lambda_{\phi ss} \phi S^2, \\
\mathcal{L}_V &= \lambda_{hvv} h V_\mu V^\mu + \lambda_{\phi vv} \phi V_\mu V^\mu,
\end{aligned} \tag{3.9}$$

where q stands for quarks and

$$\begin{aligned}
\lambda_{hss} &= -\frac{1}{2} (\nu_1 \cos \alpha \lambda_{HS} - \nu_2 \sin \alpha \lambda_{\phi S}), \\
\lambda_{\phi ss} &= -\frac{1}{2} (\nu_2 \cos \alpha \lambda_{\phi S} + \nu_1 \sin \alpha \lambda_{HS}), \\
\lambda_{hvv} &= -\sin \alpha g^2 \nu_2, \\
\lambda_{\phi vv} &= +\cos \alpha g^2 \nu_2.
\end{aligned} \tag{3.10}$$

DM scattering on nuclei have a characteristic energy scale of the order of 1 GeV and very low momentum exchange between the DM and the nucleon. On the other hand, the low DM velocity allows to consider this process in the nonrelativistic limit. Therefore, the scattering of DM with nucleons can be described by effective four field interactions between the DM and the SM quarks. After integrating the scalar mediators out, the low-energy 5-dimensional effective interaction of the DM with quarks will be

$$\begin{aligned}
\mathcal{L}_{S-q} &= \alpha_s S^2 \sum_q m_q \bar{q}q, \\
\mathcal{L}_{V-q} &= \alpha_v V_\mu V^\mu \sum_q m_q \bar{q}q,
\end{aligned} \tag{3.11}$$

where

$$\begin{aligned}
\alpha_s &= \frac{\lambda_{HS}}{2} \left(\frac{\cos^2 \alpha}{M_h^2} + \frac{\sin^2 \alpha}{M_\phi^2} \right) - \frac{\lambda_{\phi S} \cos^2 \alpha}{2} \left(\frac{1}{M_h^2} - \frac{1}{M_\phi^2} \right), \\
\alpha_v &= g^2 \cos^2 \alpha \left(\frac{1}{M_h^2} - \frac{1}{M_\phi^2} \right).
\end{aligned} \tag{3.12}$$

From this, it is possible to obtain effective interactions between the DM particle and a nucleon which gives DM-Nucleon cross section of scalar DM and vector DM [95]

$$\begin{aligned}
\sigma_s &= \alpha_s^2 \frac{M_N^4}{\pi(M_N + M_S)^2} f_N^2, \\
\sigma_v &= \alpha_v^2 \frac{M_N^4}{\pi(M_N + M_V)^2} f_N^2,
\end{aligned} \tag{3.13}$$

where M_N is the nucleon mass and $f_N = 0.3$ parametrizes the Higgs-Nucleon coupling.

The Higgs portal scattering that we discussed here led to spin independent interactions of the DM with nuclei. Some of the present constraints on DM-Nucleon spin independent interactions come from the world leader experiments, such as LUX [86],

PandaX-II [87] and XENON1T [88]. Finally, the DARWIN experiment [96], with sensitivity close to the irreducible background coming from scattering of SM neutrinos on nucleons (the so-called neutrino floor [89]), would be the ultimate DM detector. In Section 5, we constrain the model with the results of the PandaX-II experiment [87] which set an upper limit on the spin-independent WIMP-Nucleon cross section with the lowest exclusion at $M_{DM} = 40$ GeV:

$$\text{PandaX-II: } \sigma_{\text{DM-N}} \lesssim 8.6 \times 10^{-47} \text{ cm}^3. \quad (3.14)$$

Note that in above constraint, it is assumed that the local DM density is only provided by one DM specie. However, in our scenario both scalar and vector DM contribute to the local DM density. Assuming that the contribution of each DM candidates to the local DM density is the same as their contribution to the relic density, many authors constrain the rescaled DM-Nucleon cross sections, i.e., $\xi_S \sigma_s$ and $\xi_V \sigma_v$, with experimental results. However, both DM candidates contribute the DM signatures and one must combine both signatures. For the large DM mass case, where DM energy is much larger than detector threshold energy, the statistical combination is easy and the direct detection constraint reads [90]

$$\xi_S \frac{\sigma_s}{M_S} + \xi_V \frac{\sigma_v}{M_V} \lesssim \frac{\sigma}{M} \Big|_{\text{PandaX-II}}, \quad (3.15)$$

where

$$\frac{\sigma}{M} \Big|_{\text{PandaX-II}} \simeq 0.001 \frac{\text{zb}}{\text{GeV}}, \quad (3.16)$$

for $M \gtrsim 40$ GeV.

We have depicted DM-Nucleon cross section as a function of free parameters of the model in figure 5. Again, $\lambda_{\phi S}$ is irrelevant in vector DM phenomenology, e.g., σ_v . In all diagrams there are some dips where α_s or α_v vanishes. According to eq. (3.12), If $\lambda_{HS} = 0$, then we expect that dips occur at the same place where $M_h \simeq M_\varphi$. But, in general, the dips occur at different places as we see in figure 5. Another interesting feature is the double dips of σ_v in (d) diagram of figure 5. If we solve $\alpha_v = 0$ ($\Rightarrow M_h = M_\varphi$) to find M_V , we will find two solutions corresponding these double dips.

In our model, indirect detection limits are not competitive with the ones from direct detection and we will not explicitly discuss them here.

4 Electroweak phase transition

In order to study the electroweak phase transition in our model, we need to construct the effective potential. In our scenario, the effective potential is a function of the scalar field φ and temperature T . As the Universe cools down, the VEV varies from $\langle \varphi \rangle = 0$ to $\langle \varphi \rangle = \nu \neq 0$. In the following subsections we derive 1-loop effective potential and study GWs during the cosmological phase transition.

4.1 One-loop effective potential

The effective potential were initially studied at 1-loop level by Coleman and Weinberg [84]. A few years later, Gildener and Weinberg, presented their formulation for a scale invariant theory with many scalar fields [97]. As we discussed in Sec. 2, along the flat

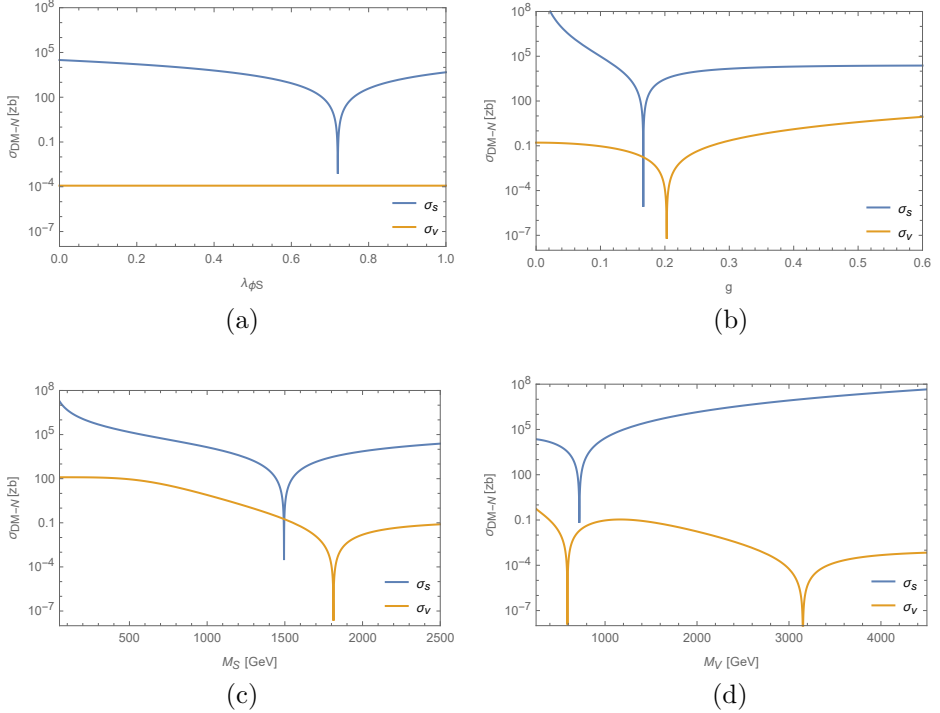


Figure 5: Variation of DM-Nucleon spin-independent cross section respect to parameter space. In all digrams the fixed parameters are: $M_S = 1800 \text{ GeV}$, $M_V = 600 \text{ GeV}$, $g = 0.2$, $\lambda_{\phi S} = 0.5$.

direction, the tree-level potential is zero, therefore, 1-loop corrections are dominated. The 1-loop effective potential at zero temperature is given by

$$V^{1-loop}(\varphi) = a\varphi^4 + b\varphi^4 \ln \frac{\varphi^2}{\Lambda^2}, \quad (4.1)$$

where

$$a = \frac{1}{64\pi^2\nu^4} \sum_{k=1}^n g_k M_k^4 \left(\ln \frac{M_k^2}{\nu^2} - C_k \right),$$

$$b = \frac{1}{64\pi^2\nu^4} \sum_{k=1}^n g_k M_k^4, \quad (4.2)$$

and Λ is the renormalization group (RG) scale. The other parameters are: $C_k = 3/2$ ($5/6$) for scalars/spinors (vectors), M_k for the measured mass of particles, and g_k for the number of degrees of freedom of the particle k (it is positive for bosons and negative for fermions). In order to have a non-zero VEV, the potential (4.1) should have a minimum

at $\varphi \neq 0$:

$$\begin{aligned} \left. \frac{dV^{1-loop}}{d\varphi} \right|_{\langle\varphi\rangle\neq 0} &= 0, \\ \left. \frac{d^2V^{1-loop}}{d\varphi^2} \right|_{\langle\varphi\rangle\neq 0} &> 0, \end{aligned} \quad (4.3)$$

which leads to

$$\langle\varphi\rangle = \nu = \Lambda e^{-(\frac{a}{2b} + \frac{1}{4})} \quad \text{and} \quad b > 0. \quad (4.4)$$

Considering both eq. (4.1) and eq. (4.4) one can substitute RG scale Λ and find a final expression for the 1-loop potential in terms of b coefficient and the true vacuum expectation value ν :

$$V^{1-loop}(\varphi) = b\varphi^4 \left(\ln \frac{\varphi^2}{\nu^2} - \frac{1}{2} \right), \quad (4.5)$$

and for the mass of φ we have $M_\varphi^2 = 8b\nu^2$ which gives eq. (2.7). Vacuum stability of a model depends on the behavior of the effective potential. If the vacuum of the effective potential is a global minimum, then the vacuum is absolutely stable. Vacuum stability up to Planck scale puts constraint on the parameters of models. After the discovery of 125 GeV Higgs boson at the LHC, we know that for SM the vacuum is not stable if no new physics is assumed (for a brief review of vacuum stability in SM see [98]). In conformal models tree-level potential is zero along flat direction and 1-loop contribution determines the behavior of the effective potential. According to conditions (4.3), the effective potential (4.5) has global minimum if $b > 0$. To fulfill this condition, considering eq. (4.2), we need new bosonic degrees of freedom with constrained masses. Albeit, for full treatment of vacuum stability, one should obtain one-loop β -functions and solve renormalization group equations (RGEs) in order to derive running coupling constants (see, e.g., [99, 100] where classically scale-invariant non-Abelian extensions of the SM are constructed satisfying perturbativity and stability up to the Planck scale.)

Apart from 1-loop zero-temperature potential (4.5), the 1-loop corrections at finite temperature also contribute to the effective potential which is given by [101]

$$V_{T\neq 0}^{1-loop}(\varphi, T) = \frac{T^4}{2\pi^2} \sum_{k=1}^n g_k J_{B,F} \left(\frac{M_k \varphi}{\nu T} \right), \quad (4.6)$$

where $J_{B,F}$ are thermal functions:

$$J_{B,F}(x) = \int_0^\infty dy y^2 \ln \left(1 \mp e^{-\sqrt{y^2+x^2}} \right). \quad (4.7)$$

We approximate thermal functions $J_B(x)$ and $J_F(x)$ in terms of modified Bessel functions of the second kind, $K_2(x)$,

$$\begin{aligned} J_B(x) &\simeq - \sum_{k=1}^3 \frac{1}{k^2} x^2 K_2(kx), \\ J_F(x) &\simeq - \sum_{k=1}^2 \frac{(-1)^k}{k^2} x^2 K_2(kx), \end{aligned} \quad (4.8)$$

which is a good approximation both in high and low temperature regimes [61]. We also consider resummed daisy graphs contribution given by [102]

$$V_{\text{daisy}}(\varphi, T) = \sum_{k=1}^n \frac{g_k T^4}{12\pi} \left(\left(\frac{M_k \varphi}{\nu T} \right)^3 - \left(\left(\frac{M_k \varphi}{\nu T} \right)^2 + \frac{\Pi_k(T)}{T^2} \right)^{3/2} \right), \quad (4.9)$$

where the sum runs only over scalar bosons and longitudinal degrees of freedom of the gauge bosons¹. The thermal masses in (4.9), $\Pi_k(T)$, are given by

$$\begin{aligned} \Pi_{h/\varphi} &= \frac{T^2}{24} \begin{pmatrix} \frac{1}{2}(9g_{\text{SM}}^2 + 3g_{\text{SM}}^{\prime 2}) + 6\lambda_t^2 + \lambda_{H\phi} + 6\lambda_H + \lambda_{HS} & 0 \\ 0 & 6g^2 + \lambda_{H\phi} + 6\lambda_\phi + \lambda_{\phi S} \end{pmatrix}, \\ \Pi_S &= \frac{T^2}{24} (\lambda_{HS} + 6\lambda_S + \lambda_{\phi S}), \quad \Pi_V = \frac{2}{3} g^2 T^2, \\ \Pi_W &= \frac{11}{6} g_{\text{SM}}^2 T^2, \quad \Pi_{Z/\gamma} = \frac{11}{6} \begin{pmatrix} g_{\text{SM}}^2 & 0 \\ 0 & g_{\text{SM}}^{\prime 2} \end{pmatrix} T^2. \end{aligned} \quad (4.10)$$

Finally, our effective potential contains Gildener-Weinberg term (4.5) and finite-temperature contributions (4.6) and (4.9):

$$V_{\text{eff}}(\varphi, T) = V^{1\text{-loop}}(\varphi) + V_{T \neq 0}^{1\text{-loop}}(\varphi, T) + V_{\text{daisy}}(\varphi, T). \quad (4.11)$$

In our calculations, in order to get $V_{\text{eff}}(0, T) = 0$ at all temperatures, we subtract a constant term from potential: $V_{\text{eff}}(\varphi, T) \rightarrow V_{\text{eff}}(\varphi, T) - V_{\text{eff}}(0, T)$. Having potential (4.11), now we are ready to study phase transition.

4.2 First order phase transition and gravitational waves

The first order phase transitions in the early Universe leave imprints in GWs which could be detected in the future. Many beyond Standard Models predict a first-order phase transition at the electroweak scale. This transition also provides an explanation for the matter-antimatter asymmetry in our Universe. In the first order phase transition, just below the critical temperature, the Universe goes from a metastable false vacuum into a stable true vacuum, through a process of bubble nucleation, growth, and merger. Such a first-order phase transition may occur in the early Universe and naturally produces GWs [73–77]. In the following we will study the dynamics of first-order phase transition and search for the parameter points of our model that can cause such transitions.

The effective potential (4.11), at some critical temperature T_C , have two degenerate minima separated by a high barrier: one in $\varphi = 0$ and the other in $\varphi = \nu_C \neq 0$:

$$\begin{aligned} V_{\text{eff}}(0, T_C) &= V_{\text{eff}}(\nu_C, T_C), \\ \left. \frac{dV_{\text{eff}}(\varphi, T_C)}{d\varphi} \right|_{\varphi=\nu_C} &= 0. \end{aligned} \quad (4.12)$$

By solving these two equations, one can obtain ν_C and T_C . Although, all independent parameters of the model contribute in the effective potential, we find that daisy term is

¹For the magnitude of theoretical uncertainties in perturbative calculations of first-order phase transitions, including usual daisy-resummed approach see [103, 104]

negligible compared to other terms, therefore $\lambda_{\phi S}$ and λ_S are irrelevant and dynamic of the phase transition only depends on M_S, M_V , and g . In figure 6, we have depicted ν_C and T_C as a function of free parameters of our model.

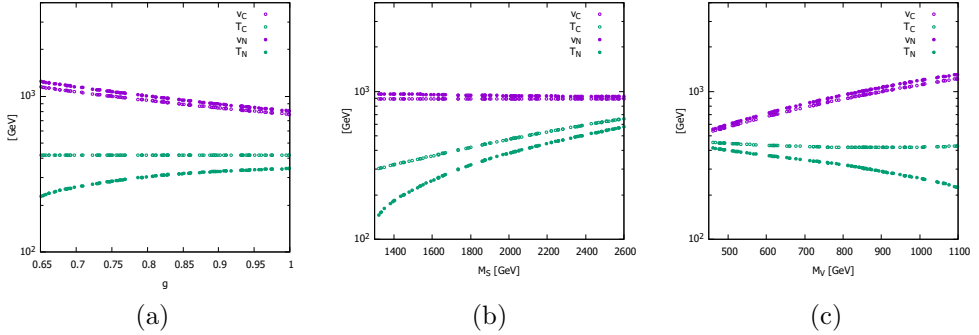


Figure 6: Variation of ν_C and T_C (ν_N and T_N) respect to parameter space. In all digrams the fixed parameters are: $M_S = 1800$ GeV , $M_V = 800$ GeV , $g = 0.85$.

Above the critical temperature $\varphi = 0$ is the true vacuum and the symmetry is not broken. As the Universe cools down, the temperature drops below the critical one and we expect a phase transition from the false vacuum $\varphi = 0$ to the true vacuum $\varphi \neq 0$ via thermal tunneling at finite temperature. Once this transition has happened, bubbles of the broken phase form in the sea of the symmetric phase and spread throughout the universe converting the false vacuum into the true one.

The bubbles formation starts after the temperature drops below T_C , however it goes sufficiently fast to fill the universe with bubbles of the new phase only at some lower temperature, the nucleation temperature T_N , where the corresponding euclidean action is $S_E = S_3(T_N)/T_N \sim 140^2$. The function $S_3(T)$ is the three-dimensional Euclidean action for a spherical symmetric bubble given by

$$S_3(T) = 4\pi \int_0^\infty dr r^2 \left(\frac{1}{2} \left(\frac{d\varphi}{dr} \right)^2 + V_{eff}(\varphi, T) \right), \quad (4.13)$$

where φ satisfies the differential equation which minimizes S_3 :

$$\frac{d^2\varphi}{dr^2} + \frac{2}{r} \frac{d\varphi}{dr} = \frac{dV_{eff}(\varphi, T)}{d\varphi}, \quad (4.14)$$

with the boundary conditions:

$$\left. \frac{d\varphi}{dr} \right|_{r=0} = 0, \quad \text{and} \quad \varphi(r \rightarrow \infty) = 0. \quad (4.15)$$

In order to solve eq. (4.14) and find the Euclidean action (4.13), we have used `AnyBubble` package [106]. In figure 6, we have also depicted ν_N and T_N as a function of g, M_S , and M_V .

The stochastic GW background produced by strong first-order electroweak phase transitions comes from three contributions:

²This condition at the vacuum-dominated period should be treated more carefully (see, e.g., [105]).

- bubble walls collisions and shocks in the plasma,
- sound waves to the stochastic background after bubble collisions but before expansion has dissipated the kinetic energy in the plasma, and
- turbulence forming after bubble collisions.

These three processes may coexist, and each one contributes to the stochastic GW background:

$$\Omega_{\text{GW}}h^2 \simeq \Omega_{\text{coll}}h^2 + \Omega_{\text{sw}}h^2 + \Omega_{\text{turb}}h^2. \quad (4.16)$$

All of the above contributions are controlled by four thermal parameters:

- the nucleation temperature, T_N ,
- the strength parameter which is the ratio of the free energy density difference between the true and false vacuum and the total energy density, α ,

$$\alpha = \frac{\Delta \left(V_{\text{eff}} - T \frac{\partial V_{\text{eff}}}{\partial T} \right) \Big|_{T_N}}{\rho_*}, \quad (4.17)$$

where ρ_* is

$$\rho_* = \frac{\pi^2 g_* T_N^4}{30}, \quad (4.18)$$

- the inverse time duration of the phase transition, β ,

$$\frac{\beta}{H_*} = T_N \frac{d}{dT} \left(\frac{S_3(T)}{T} \right) \Big|_{T_N}, \quad (4.19)$$

- and the velocity of the bubble wall, v_w , which is anticipated to be close to 1 for the strong transitions [107].

In figure 7, we have depicted α and β/H_* as a function of independent parameters of our model. For the chosen parameters we found $\alpha \sim 10^{-2} - 10^{-1}$ and $\beta/H_* \sim 10^2 - 10^3$.

In the process of the GW production, first the bubbles of the stable phase collide and merge. This stage is subdominant compared to the subsequent stages of GW production, unless the bubbles grow as large as the Hubble length itself. The bubble collision contribution is given by [108]

$$\Omega_{\text{coll}}(f)h^2 = 1.67 \times 10^{-5} \left(\frac{\beta}{H_*} \right)^{-2} \left(\frac{\kappa\alpha}{1+\alpha} \right)^2 \left(\frac{g_*}{100} \right)^{-\frac{1}{3}} \left(\frac{0.11 v_w^3}{0.42 + v_w^2} \right) S_{\text{coll}}, \quad (4.20)$$

where S_{coll} parametrises the spectral shape given by

$$S_{\text{coll}} = \frac{3.8 (f/f_{\text{coll}})^{2.8}}{2.8 (f/f_{\text{coll}})^{3.8} + 1}, \quad (4.21)$$

with

$$f_{\text{coll}} = 1.65 \times 10^{-5} \left(\frac{0.62}{v_w^2 - 0.1v_w + 1.8} \right) \left(\frac{\beta}{H_*} \right) \left(\frac{T_N}{100} \right) \left(\frac{g_*}{100} \right)^{1/6} \text{ Hz}. \quad (4.22)$$

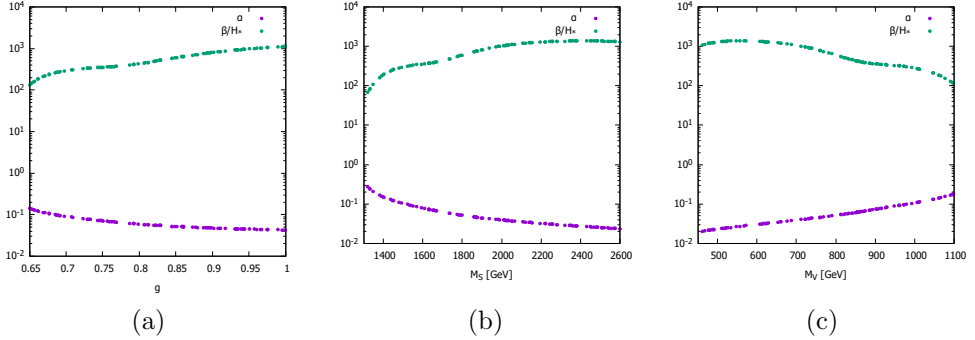


Figure 7: Variation of α and β/H_* respect to parameter space. In all digrams the fixed parameters are: $M_S = 1800 \text{ GeV}$, $M_V = 800 \text{ GeV}$, $g = 0.85$.

After the bubble collision, the shells of fluid kinetic energy continue to expand into the plasma as sound waves. These different waves overlap and source the dominant contribution to the GW signal which is given by³ [110]

$$\Omega_{\text{sw}}(f)h^2 = 2.65 \times 10^{-6} \left(\frac{\beta}{H_*} \right)^{-1} \left(\frac{\kappa_v \alpha}{1 + \alpha} \right)^2 \left(\frac{g_*}{100} \right)^{-\frac{1}{3}} v_w S_{\text{sw}}. \quad (4.23)$$

The spectral shape of S_{sw} is

$$S_{\text{sw}} = (f/f_{\text{sw}})^3 \left(\frac{7}{3(f/f_{\text{sw}})^2 + 4} \right)^{3.5}, \quad (4.24)$$

where

$$f_{\text{sw}} = 1.9 \times 10^{-5} \frac{1}{v_w} \left(\frac{\beta}{H_*} \right) \left(\frac{T_N}{100} \right) \left(\frac{g_*}{100} \right)^{1/6} \text{ Hz}. \quad (4.25)$$

Finally, the last stage is the turbulent phase which its contribution to the GW spectrum is given by [111]

$$\Omega_{\text{turb}}(f)h^2 = 3.35 \times 10^{-4} \left(\frac{\beta}{H_*} \right)^{-1} \left(\frac{\kappa_{\text{turb}} \alpha}{1 + \alpha} \right)^{3/2} \left(\frac{g_*}{100} \right)^{-\frac{1}{3}} v_w S_{\text{turb}}, \quad (4.26)$$

where

$$S_{\text{turb}} = \frac{(f/f_{\text{turb}})^3}{(1 + 8\pi f/h_*) (1 + f/f_{\text{turb}})^{11/3}}, \quad (4.27)$$

and

$$f_{\text{turb}} = 2.27 \times 10^{-5} \frac{1}{v_w} \left(\frac{\beta}{H_*} \right) \left(\frac{T_N}{100} \right) \left(\frac{g_*}{100} \right)^{1/6} \text{ Hz}. \quad (4.28)$$

³A recent study in [109] suggests the existence of a suppression factor for the sound wave contribution due to the finite lifetime of the GWs. The factor takes an asymptotic value of 1 for a very long lifetime.

In eq. (4.27), the parameter h_* is the value of the inverse Hubble time at GW production, redshifted to today,

$$h_* = 1.65 \times 10^{-5} \left(\frac{T_N}{100} \right) \left(\frac{g_*}{100} \right)^{1/6}. \quad (4.29)$$

In the formulas of GW spectrum we have used [112, 113]

$$\begin{aligned} \kappa &= \frac{1}{1 + 0.715 \alpha} \left(0.715 \alpha + \frac{4}{27} \sqrt{\frac{3\alpha}{2}} \right), \\ \kappa_v &= \frac{\alpha}{0.73 + 0.083 \sqrt{\alpha + \alpha}}, \quad \kappa_{\text{turb}} = 0.05 \kappa_v, \end{aligned} \quad (4.30)$$

where the parameters κ , κ_v , and κ_{turb} denote the fraction of latent heat that is transformed into gradient energy of the Higgs-like field, bulk motion of the fluid, and MHD turbulence, respectively.

5 Results

After having studied DM phenomenology and electroweak phase transition of our two-component DM model in the previous sections, we will now concentrate on the question of whether it is feasible to correctly reproduce the known features of DM and first order phase transition at the same time. On the DM side, we have relic density constraint as well as the upper bound of DM-Nucleon cross section obtained in direct detection experiments. On the other hand, we are looking for strong first order phase transition which leads to GW production at the early Universe. Obviously, the above requirements will impose constraints on the parameter space of the model, which is the subject of the present section.

In order to obtain the parameter space consistent with DM relic density (see eq. (3.6)) and direct detection constraint (see eq. (3.15)), we should scan over four independent parameters of the model, i.e., M_S , M_V , g , and $\lambda_{\phi S}$. To do so, regarding the strong constraint on DM-Nucleon cross section, we first obtain \bar{g} and $\bar{\lambda}$ using the following equations

$$\alpha_v \Big|_{g=\bar{g}} = 0, \quad \alpha_s \Big|_{\lambda_{\phi S}=\bar{\lambda}} = 0. \quad (5.1)$$

Considering eqs. (2.7), (2.8), (3.8) and (3.12), the solutions are given by

$$\begin{aligned} \bar{g}(M_V, M_S) &= \frac{M_V}{\sqrt{\frac{\sum_{k=1}^n g_k M_k^4}{8\pi^2 M_h^2} - \nu_1^2}}, \\ \bar{\lambda}(M_V, M_S, g) &= \frac{2M_S^2 (\sin^2 \alpha M_h^2 + \cos^2 \alpha M_\varphi^2)}{\nu^2 \cos^2 \alpha M_\varphi^2}. \end{aligned} \quad (5.2)$$

Now, looking for the correct value of DM relic density (3.6) and regarding perturbativity constraints (all couplings $< 4\pi$), we scan over random values of M_S and M_V , while we choose $0.9 \bar{g} < g < 1.1 \bar{g}$ and $0.9 \bar{\lambda} < \lambda_{\phi S} < 1.1 \bar{\lambda}$. In this way, according to eq. (3.13), we restrict ourselves to the small values of σ_s and σ_v which can possibly evade the direct

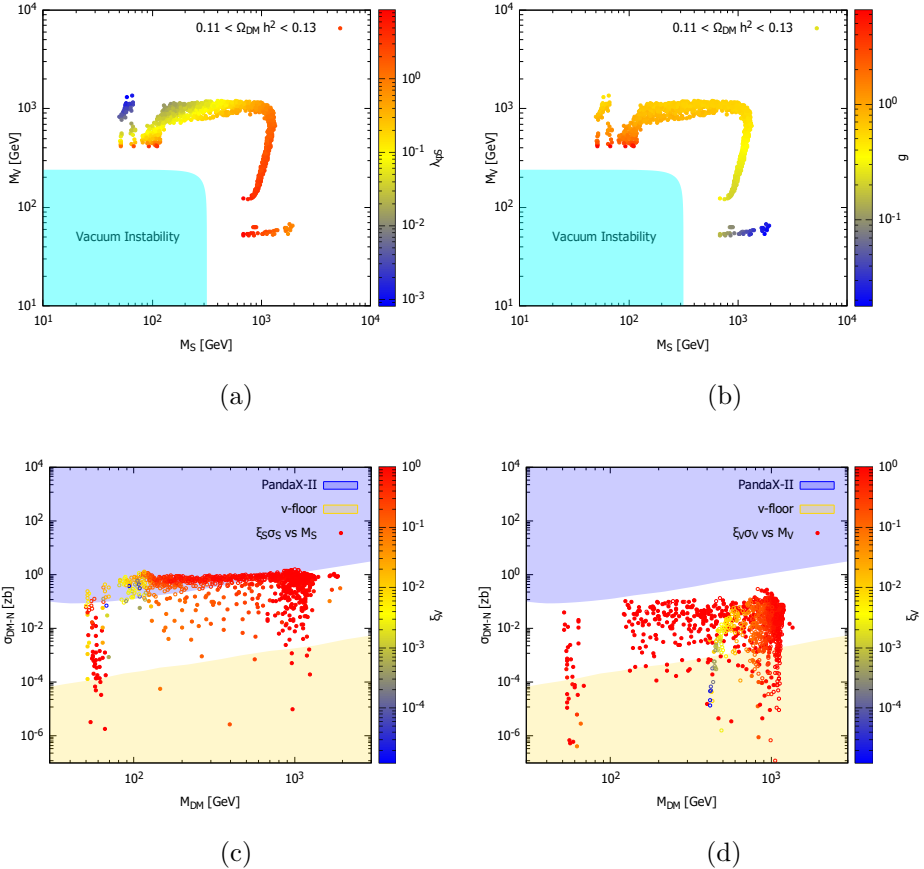


Figure 8: (a) and (b): parameter space consistent with DM Relic density. Cyan region is not allowed because in this region $M_\varphi^2 < 0$ (see eq. 2.7) and we do not have a global vacuum. (c) and (d): Rescaled DM-Nucleon cross section for the parameter space already constrained by DM relic density. Hollow circles are excluded by direct detection constraint (3.15).

detection constraint (3.15). According to this strategy, we obtain DM relic density for $40 \text{ GeV} \lesssim M_{DM} \lesssim 2000 \text{ GeV}$.

In figure 8 (a) and (b), the parameter space consistent with DM relic density is obtained based on our strategy. In (c) and (d), for these parameters, rescaled DM-Nucleon cross sections, i.e., $\xi_S \sigma_S$ and $\xi_V \sigma_V$, are also depicted. As we see, there are some points between the PandaX-II direct detection bound and the neutrino floor which can be probed in the future direct detection experiments. Although DM relic density and direct detection experiments restrict the model, there are some parts of the parameter space which is not excluded yet. In figure 8 (c) and (d), we have also depicted the fraction of vector DM, ξ_V . As we see, for some scatter points, vector DM is dominated, while for the other points DM mostly consists of scalar DM. Note that, although our strategy strongly restricts the parameter space in order to get unconstrained DM-Nucleon cross

section, still there are some points which violate direct detection constraint (3.15). These points are depicted with hollow circles and they should be excluded even when they are below the upper bound of Pandax-II. Therefore, considering $\xi_S\sigma_s$ and $\xi_V\sigma_v$ separately is not enough and in order to constrain two component DM models by direct detection experiments, one should combine both signatures.

Now looking for the first order electroweak phase transition and GW, we scan over the parameter space once more. In accordance with the DM results, we choose the same range of the parameters as figure 8. The result is shown in figure 9.

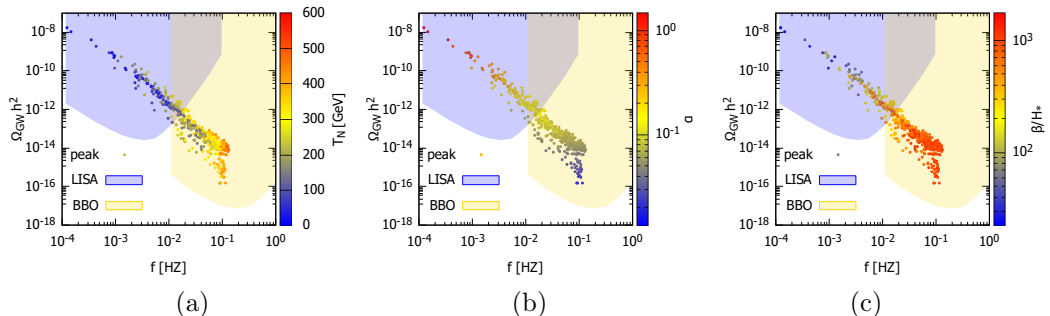


Figure 9: The peak of GW spectrum against frequency. LISA and BBO sensitivities are also depicted.

In study of phase transition and GW, the relevant parameters are M_S, M_V , and g . We found that for around 14 percent of the parameter space scanned here, first order phase transition can occur, generating a stochastic background of GWs. Most peaks of the GW spectrum are detectable by LISA and BBO detectors⁴.

So far, we have studied DM phenomenology and phase transition separately. Now we consider both aspects simultaneously which gives us figure 10. In this figure, we have used the scatter points already obtained in the study of DM phenomenology, and saw if they also produce first order phase transition and GWs. In general, the DM freeze-out temperature $T_F \sim M_{DM}/20$ may be greater than nucleation temperature T_N in some parameter points. In this case, as the phase transition is not completed, the freeze-out can be affected. For phenomenology of a late phase transition see [117]. However, for the parameter points in figure 10, we have compared freeze-out temperature with nucleation temperature and find out $T_F < T_N$ where $T_F \sim \max(M_S, M_V)/20$. Therefore, this issue does not affect our result and the DM properties would not be modified between T_F and the present day, at least for the parameter space considered in figure 10 (where $0.31 \lesssim T_F/T_N \lesssim 0.47$).

As figure 10 implies, for some points in the parameter space, the model is consistent with DM constraints, while at the same time generates first order electroweak phase transition and GWs detectable by LISA and BBO. To be more explicit, we have chosen two benchmark points given in table 1. In this table all relevant quantities, including independent parameters of the model, DM properties, and phase transition parameters, are given.

⁴For a new type of sensitivity curves for gravitational-wave signals from cosmological first order phase transitions for LISA and BBO see [114–116]

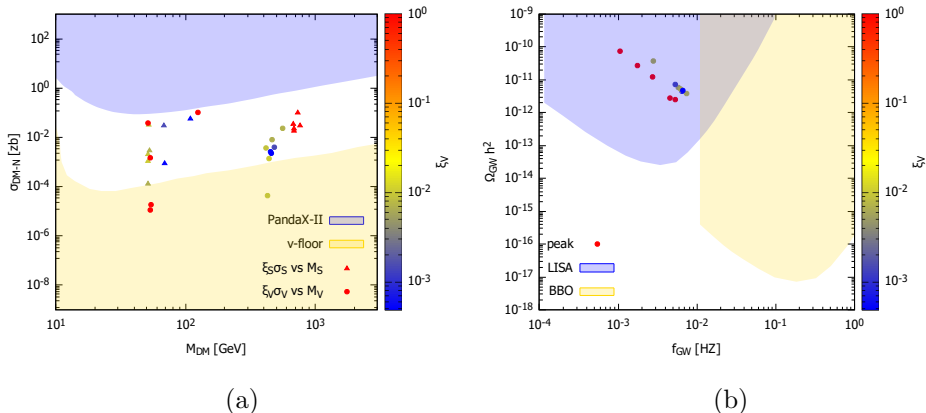


Figure 10: (a): Rescaled DM-Nucleon cross section VS DM mass. The scatter points are already consistent with DM relic density (3.6) and direct detection (3.15) constraints. (b): GW peak VS frequency for the same points of the parameter space.

#	$\lambda_{\phi S}$	g	M_S (GeV)	M_V (GeV)	M_φ (GeV)
1	0.036	1.469	52.37	559.4	132.3
2	5.491	0.118	761.0	53.78	124.4

#	$\Omega_S h^2$	$\Omega_V h^2$	$\Omega_{DM} h^2$	$\xi_S \sigma_S$ (zb)	$\xi_V \sigma_V$ (zb)
1	1.09×10^{-1}	7.72×10^{-4}	1.10×10^{-1}	2.93×10^{-3}	2.29×10^{-2}
2	1.00×10^{-3}	1.12×10^{-1}	1.13×10^{-1}	2.99×10^{-2}	1.83×10^{-5}

#	T_C (GeV)	T_N (GeV)	α	β/H_*	$(\Omega_{\text{GW}} h^2)_{\text{max}}$
1	135.9	78.19	0.257	187.2	3.71×10^{-11}
2	161.0	81.14	0.234	68.72	7.59×10^{-11}

Table 1: Two benchmark points with DM and phase transition parameters.

For these benchmark points, the GW spectrum is depicted in figure 11. For both benchmark points, around the peak, the dominated contribution of GW signal is sound wave. For the first benchmark point, scalar DM is dominant, while for the second one, vector DM makes most of DM relic density. The peak of the GW spectrum for both benchmark points falls within the observational window of LISA.

Finally, we should mention that sound wave contribution dominates for all scatter points in figure 10 and it is almost indistinguishable from the sum of the three sources, at least around the GW peak. However, far from the peak, this is not necessarily the case. For example, after the fracture of the first benchmark curve around 0.1 HZ, the bubble collision contribution will be dominated.

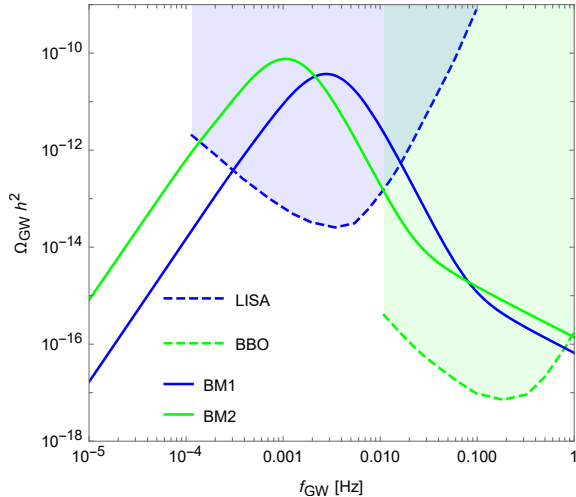


Figure 11: GW spectrum for benchmark points of the table 1.

6 Conclusion

In this work we studied a two-component DM model as an extension of the SM with classical scale symmetry. It realizes electroweak symmetry breaking through Gildener-Weinberg mechanism and gives a natural solution to the hierarchy problem. The model consists three new fields: a real scalar, a complex scalar, and a vector field which two of them, the real scalar field and vector field, can play the role of DM. Our two-component DM model is obtained by adding them to the SM via the Higgs-portal. The Boltzmann equations for both DM components were solved numerically and in order to determine a region of parameter space that is consistent with Planck and PandaX-II data a scan over four dimensional parameter space was performed.

After introducing the model and investigating DM phenomenology, we focused on the phase transition dynamics. With the aim of exploring the nature and the strength of the electroweak phase transition, the full finite-temperature effective potential of the model at one loop level has been obtained. Despite the absence of a barrier in the zero-temperature potential, it was demonstrated that the finite-temperature effects induce a barrier between the symmetric and the broken phase vacua, and thereby give rise to a first-order electroweak phase transition which can generate GWs.

The spectrum of these GWs can be described in terms of only four properties: the bubble nucleation temperature T_N , the strength parameter α , the transition rate parameter β , and the bubble wall speed v_w . These are all computable from the underlying particle physics model and therefore are functions of the independent parameters of our model. The space missions such as LISA and BBO could detect these GWs if the phase transition took place at scale of electroweak symmetry-breaking. LISA and BBO are particle physics experiments, as well as astrophysical observatories. Albeit, much should be done to realize the goal of making LISA into a particle physics experiment to complement the Large Hadron Collider (LHC). On the other hand, although continuing efforts at the LHC will be able to examine some of the beyond Standard Models, there remain many

that cannot be probed through collider experiments on a timescale as good as LISA and BBO, if at all.

Our results indicate the model can survive DM relic density and direct detection constraints, while at the same time produce GWs during the first order electroweak phase transition. A positive GW signal at LISA and BBO would most likely point toward new physics at the TeV scale such as the classically scale invariant potential studied here.

References

- [1] G. Bertone and D. Hooper, *History of dark matter*, *Rev. Mod. Phys.* **90** (2018) 045002 [[arXiv:1605.04909](#)] [[INSPIRE](#)].
- [2] K. M. Zurek, *Multi-Component Dark Matter*, *Phys. Rev. D* **79** (2009) 115002 [[arXiv:0811.4429](#)] [[INSPIRE](#)].
- [3] S. Profumo, K. Sigurdson and L. Ubaldi, *Can we discover multi-component WIMP dark matter?*, *JCAP* **12** (2009) 016 [[arXiv:0907.4374](#)] [[INSPIRE](#)].
- [4] M. Aoki, M. Duerr, J. Kubo and H. Takano, *Multi-Component Dark Matter Systems and Their Observation Prospects*, *Phys. Rev. D* **86** (2012) 076015 [[arXiv:1207.3318](#)] [[INSPIRE](#)].
- [5] A. Biswas, D. Majumdar, A. Sil and P. Bhattacharjee, *Two Component Dark Matter : A Possible Explanation of 130 GeV γ - Ray Line from the Galactic Centre*, *JCAP* **12** (2013) 049 [[arXiv:1301.3668](#)] [[INSPIRE](#)].
- [6] P.-H. Gu, *Multi-component dark matter with magnetic moments for Fermi-LAT gamma-ray line*, *Phys. Dark Univ.* **2** (2013) 35 [[arXiv:1301.4368](#)] [[INSPIRE](#)].
- [7] M. Aoki, J. Kubo and H. Takano, *Two-loop radiative seesaw mechanism with multicomponent dark matter explaining the possible γ excess in the Higgs boson decay and at the Fermi LAT*, *Phys. Rev. D* **87** (2013) 116001 [[arXiv:1302.3936](#)] [[INSPIRE](#)].
- [8] Y. Kajiyama, H. Okada and T. Toma, *Multicomponent dark matter particles in a two-loop neutrino model*, *Phys. Rev. D* **88** (2013) 015029 [[arXiv:1303.7356](#)] [[INSPIRE](#)].
- [9] L. Bian, R. Ding and B. Zhu, *Two Component Higgs-Portal Dark Matter*, *Phys. Lett. B* **728** (2014) 105 [[arXiv:1308.3851](#)] [[INSPIRE](#)].
- [10] S. Bhattacharya, A. Drozd, B. Grzadkowski and J. Wudka, *Two-Component Dark Matter*, *JHEP* **10** (2013) 158 [[arXiv:1309.2986](#)] [[INSPIRE](#)].
- [11] C.-Q. Geng, D. Huang and L.-H. Tsai, *Imprint of multicomponent dark matter on AMS-02*, *Phys. Rev. D* **89** (2014) 055021 [[arXiv:1312.0366](#)] [[INSPIRE](#)].
- [12] S. Esch, M. Klasen and C. E. Yaguna, *A minimal model for two-component dark matter*, *JHEP* **09** (2014) 108 [[arXiv:1406.0617](#)] [[INSPIRE](#)].

- [13] K. R. Dienes, J. Kumar, B. Thomas and D. Yaylali, *Dark-Matter Decay as a Complementary Probe of Multicomponent Dark Sectors*, *Phys. Rev. Lett.* **114** (2015) 051301 [[arXiv:1406.4868](#)] [[INSPIRE](#)].
- [14] L. Bian, T. Li, J. Shu and X.-C. Wang, *Two component dark matter with multi-Higgs portals*, *JHEP* **03** (2015) 126 [[arXiv:1412.5443](#)] [[INSPIRE](#)].
- [15] C.-Q. Geng, D. Huang and C. Lai, *Revisiting multicomponent dark matter with new AMS-02 data*, *Phys. Rev. D* **91** (2015) 095006 [[arXiv:1411.4450](#)] [[INSPIRE](#)].
- [16] A. DiFranzo and G. Mohlabeng, *Multi-component Dark Matter through a Radiative Higgs Portal*, *JHEP* **01** (2017) 080 [[arXiv:1610.07606](#)] [[INSPIRE](#)].
- [17] M. Aoki and T. Toma, *Implications of Two-component Dark Matter Induced by Forbidden Channels and Thermal Freeze-out*, *JCAP* **01** (2017) 042 [[arXiv:1611.06746](#)] [[INSPIRE](#)].
- [18] A. Dutta Banik, M. Pandey, D. Majumdar and A. Biswas, *Two component WIMP-FIMP dark matter model with singlet fermion, scalar and pseudo scalar*, *Eur. Phys. J. C* **77** (2017) 657 [[arXiv:1612.08621](#)] [[INSPIRE](#)].
- [19] M. Pandey, D. Majumdar and K. P. Modak, *Two Component Feebly Interacting Massive Particle (FIMP) Dark Matter*, *JCAP* **06** (2018) 023 [[arXiv:1709.05955](#)] [[INSPIRE](#)].
- [20] D. Borah, A. Dasgupta, U. K. Dey, S. Patra and G. Tomar, *Multi-component Fermionic Dark Matter and IceCube PeV scale Neutrinos in Left-Right Model with Gauge Unification*, *JHEP* **09** (2017) 005 [[arXiv:1704.04138](#)] [[INSPIRE](#)].
- [21] J. Herrero-Garcia, A. Scaffidi, M. White and A. G. Williams, *On the direct detection of multi-component dark matter: sensitivity studies and parameter estimation*, *JCAP* **11** (2017) 021 [[arXiv:1709.01945](#)] [[INSPIRE](#)].
- [22] A. Ahmed, M. Duch, B. Grzadkowski and M. Iglicki, *Multi-Component Dark Matter: the vector and fermion case*, *Eur. Phys. J. C* **78** (2018) 905 [[arXiv:1710.01853](#)] [[INSPIRE](#)].
- [23] S. Peyman Zakeri, S. Mohammad Moosavi Nejad, M. Zakeri and S. Y. Ayazi, *A Minimal Model For Two-Component FIMP Dark Matter: A Basic Search*, *Chin. Phys. C* **42** (2018) 073101 [[arXiv:1801.09115](#)] [[INSPIRE](#)].
- [24] M. Aoki and T. Toma, *Boosted Self-interacting Dark Matter in a Multi-component Dark Matter Model*, *JCAP* **10** (2018) 020 [[arXiv:1806.09154](#)] [[INSPIRE](#)].
- [25] S. Chakraborti and P. Poulose, *Interplay of Scalar and Fermionic Components in a Multi-component Dark Matter Scenario*, *Eur. Phys. J. C* **79** (2019) 420 [[arXiv:1808.01979](#)] [[INSPIRE](#)].
- [26] N. Bernal, D. Restrepo, C. Yaguna and O. Zapata, *Two-component dark matter and a massless neutrino in a new $B - L$ model*, *Phys. Rev. D* **99** (2019) 015038 [[arXiv:1808.03352](#)] [[INSPIRE](#)].

- [27] A. Poulin and S. Godfrey, *Multicomponent dark matter from a hidden gauged $SU(3)$* , *Phys. Rev. D* **99** (2019) 076008 [[arXiv:1808.04901](#)] [[INSPIRE](#)].
- [28] J. Herrero-Garcia, A. Scaffidi, M. White and A. G. Williams, *On the direct detection of multi-component dark matter: implications of the relic abundance*, *JCAP* **01** (2019) 008 [[arXiv:1809.06881](#)] [[INSPIRE](#)].
- [29] S. Y. Ayazi and A. Mohamadnejad, *Scale-Invariant Two Component Dark Matter*, *Eur. Phys. J. C* **79** (2019) 140 [[arXiv:1808.08706](#)] [[INSPIRE](#)].
- [30] F. Elahi and S. Khatibi, *Multi-Component Dark Matter in a Non-Abelian Dark Sector*, *Phys. Rev. D* **100** (2019) 015019 [[arXiv:1902.04384](#)] [[INSPIRE](#)].
- [31] D. Borah, A. Dasgupta and S. K. Kang, *Two-component dark matter with cogenesis of the baryon asymmetry of the Universe*, *Phys. Rev. D* **100** (2019) 103502 [[arXiv:1903.10516](#)] [[INSPIRE](#)].
- [32] D. Borah, R. Roshan and A. Sil, *Minimal two-component scalar doublet dark matter with radiative neutrino mass*, *Phys. Rev. D* **100** (2019) 055027 [[arXiv:1904.04837](#)] [[INSPIRE](#)].
- [33] S. Bhattacharya, P. Ghosh, A. K. Saha and A. Sil, *Two component dark matter with inert Higgs doublet: neutrino mass, high scale validity and collider searches*, *JHEP* **03** (2020) 090 [[arXiv:1905.12583](#)] [[INSPIRE](#)].
- [34] A. Biswas, D. Borah and D. Nanda, *Type III seesaw for neutrino masses in $U(1)_{B-L}$ model with multi-component dark matter*, *JHEP* **12** (2019) 109 [[arXiv:1908.04308](#)] [[INSPIRE](#)].
- [35] D. Nanda and D. Borah, *Connecting Light Dirac Neutrinos to a Multi-component Dark Matter Scenario in Gauged $B - L$ Model*, *Eur. Phys. J. C* **80** (2020) 557 [[arXiv:1911.04703](#)] [[INSPIRE](#)].
- [36] C. E. Yaguna and O. Zapata, *Multi-component scalar dark matter from a Z_N symmetry: a systematic analysis*, *JHEP* **03** (2020) 109 [[arXiv:1911.05515](#)] [[INSPIRE](#)].
- [37] G. Bélanger, A. Pukhov, C. E. Yaguna and O. Zapata, *The Z_5 model of two-component dark matter*, *JHEP* **09** (2020) 030 [[arXiv:2006.14922](#)] [[INSPIRE](#)].
- [38] P. Van Dong, C. H. Nam and D. Van Loi, *Canonical seesaw implication for two-component dark matter*, *Phys. Rev. D* **103** (2021) 095016 [[arXiv:2007.08957](#)] [[INSPIRE](#)].
- [39] S. Khalil, S. Moretti, D. Rojas-Ciofalo and H. Waltari, *Multicomponent dark matter in a simplified E_6 SSM*, *Phys. Rev. D* **102** (2020) 075039 [[arXiv:2007.10966](#)] [[INSPIRE](#)].
- [40] A. Dutta Banik, R. Roshan and A. Sil, *Two component singlet-triplet scalar dark matter and electroweak vacuum stability*, *Phys. Rev. D* **103** (2021) 075001 [[arXiv:2009.01262](#)] [[INSPIRE](#)].

- [41] J. Hernandez-Sanchez, V. Keus, S. Moretti, D. Rojas-Ciofalo and D. Sokolowska, *Complementary Probes of Two-component Dark Matter*, [arXiv:2012.11621](#) [INSPIRE].
- [42] N. Chakrabarty, R. Roshan and A. Sil, *Two Component Doublet-Triplet Scalar Dark Matter stabilising the Electroweak vacuum*, [arXiv:2102.06032](#) [INSPIRE].
- [43] C. E. Yaguna and O. Zapata, *Two-component scalar dark matter in Z_{2n} scenarios*, *JHEP* **10** (2021) 185 [[arXiv:2106.11889](#)] [INSPIRE].
- [44] B. Díaz Sáez, P. Escalona, S. Norero and A. R. Zerwekh, *Fermion singlet dark matter in a pseudoscalar dark matter portal*, *JHEP* **10** (2021) 233 [[arXiv:2105.04255](#)] [INSPIRE].
- [45] B. Díaz Sáez, K. Möhling and D. Stöckinger, *Two Real Scalar WIMP Model in the Assisted Freeze-Out Scenario*, *JCAP* **10** (2021) 027 [[arXiv:2103.17064](#)] [INSPIRE].
- [46] K. Kajantie, M. Laine, K. Rummukainen and M. E. Shaposhnikov, *Is there a hot electroweak phase transition at $m_H \gtrsim m_W$?*, *Phys. Rev. Lett.* **77** (1996) 2887 [[hep-ph/9605288](#)] [INSPIRE].
- [47] M. Chala, G. Nardini and I. Sobolev, *Unified explanation for dark matter and electroweak baryogenesis with direct detection and gravitational wave signatures*, *Phys. Rev. D* **94** (2016) 055006 [[arXiv:1605.08663](#)] [INSPIRE].
- [48] A. Soni and Y. Zhang, *Gravitational Waves From $SU(N)$ Glueball Dark Matter*, *Phys. Lett. B* **771** (2017) 379 [[arXiv:1610.06931](#)] [INSPIRE].
- [49] R. Flauger and S. Weinberg, *Gravitational Waves in Cold Dark Matter*, *Phys. Rev. D* **97** (2018) 123506 [[arXiv:1801.00386](#)] [INSPIRE].
- [50] I. Baldes, *Gravitational waves from the asymmetric-dark-matter generating phase transition*, *JCAP* **05** (2017) 028 [[arXiv:1702.02117](#)] [INSPIRE].
- [51] W. Chao, H.-K. Guo and J. Shu, *Gravitational Wave Signals of Electroweak Phase Transition Triggered by Dark Matter*, *JCAP* **09** (2017) 009 [[arXiv:1702.02698](#)] [INSPIRE].
- [52] A. Beniwal, M. Lewicki, J. D. Wells, M. White and A. G. Williams, *Gravitational wave, collider and dark matter signals from a scalar singlet electroweak baryogenesis*, *JHEP* **08** (2017) 108 [[arXiv:1702.06124](#)] [INSPIRE].
- [53] F. P. Huang and J.-H. Yu, *Exploring inert dark matter blind spots with gravitational wave signatures*, *Phys. Rev. D* **98** (2018) 095022 [[arXiv:1704.04201](#)] [INSPIRE].
- [54] F. P. Huang and C. S. Li, *Probing the baryogenesis and dark matter relaxed in phase transition by gravitational waves and colliders*, *Phys. Rev. D* **96** (2017) 095028 [[arXiv:1709.09691](#)] [INSPIRE].

- [55] E. Madge and P. Schwaller, *Leptophilic dark matter from gauged lepton number: Phenomenology and gravitational wave signatures*, *JHEP* **02** (2019) 048 [[arXiv:1809.09110](#)] [[INSPIRE](#)].
- [56] L. Bian and Y.-L. Tang, *Thermally modified sterile neutrino portal dark matter and gravitational waves from phase transition: The Freeze-in case*, *JHEP* **12** (2018) 006 [[arXiv:1810.03172](#)] [[INSPIRE](#)].
- [57] L. Bian and X. Liu, *Two-step strongly first-order electroweak phase transition modified FIMP dark matter, gravitational wave signals, and the neutrino mass*, *Phys. Rev. D* **99** (2019) 055003 [[arXiv:1811.03279](#)] [[INSPIRE](#)].
- [58] V. R. Shajiee and A. Tofighi, *Electroweak Phase Transition, Gravitational Waves and Dark Matter in Two Scalar Singlet Extension of The Standard Model*, *Eur. Phys. J. C* **79** (2019) 360 [[arXiv:1811.09807](#)] [[INSPIRE](#)].
- [59] K. Kannike and M. Raidal, *Phase Transitions and Gravitational Wave Tests of Pseudo-Goldstone Dark Matter in the Softly Broken $U(1)$ Scalar Singlet Model*, *Phys. Rev. D* **99** (2019) 115010 [[arXiv:1901.03333](#)] [[INSPIRE](#)].
- [60] S. Y. Ayazi and A. Mohamadnejad, *Conformal vector dark matter and strongly first-order electroweak phase transition*, *JHEP* **03** (2019) 181 [[arXiv:1901.04168](#)] [[INSPIRE](#)].
- [61] A. Mohamadnejad, *Gravitational waves from scale-invariant vector dark matter model: Probing below the neutrino-floor*, *Eur. Phys. J. C* **80** (2020) 197 [[arXiv:1907.08899](#)] [[INSPIRE](#)].
- [62] K. Kannike, K. Loos and M. Raidal, *Gravitational wave signals of pseudo-Goldstone dark matter in the \mathbb{Z}_3 complex singlet model*, *Phys. Rev. D* **101** (2020) 035001 [[arXiv:1907.13136](#)] [[INSPIRE](#)].
- [63] A. Paul, B. Banerjee and D. Majumdar, *Gravitational wave signatures from an extended inert doublet dark matter model*, *JCAP* **10** (2019) 062 [[arXiv:1908.00829](#)] [[INSPIRE](#)].
- [64] B. Barman, A. Dutta Banik and A. Paul, *Singlet-doublet fermionic dark matter and gravitational waves in a two-Higgs-doublet extension of the Standard Model*, *Phys. Rev. D* **101** (2020) 055028 [[arXiv:1912.12899](#)] [[INSPIRE](#)].
- [65] D. Marfatia and P.-Y. Tseng, *Gravitational wave signals of dark matter freeze-out*, *JHEP* **02** (2021) 022 [[arXiv:2006.07313](#)] [[INSPIRE](#)].
- [66] T. Alanne, N. Benincasa, M. Heikinheimo, K. Kannike, V. Keus, N. Koivunen et al., *Pseudo-Goldstone dark matter: gravitational waves and direct-detection blind spots*, *JHEP* **10** (2020) 080 [[arXiv:2008.09605](#)] [[INSPIRE](#)].
- [67] X.-F. Han, L. Wang and Y. Zhang, *Dark matter, electroweak phase transition, and gravitational waves in the type II two-Higgs-doublet model with a singlet scalar field*, *Phys. Rev. D* **103** (2021) 035012 [[arXiv:2010.03730](#)] [[INSPIRE](#)].

- [68] Y. Wang, C. S. Li and F. P. Huang, *Complementary probe of dark matter blind spots by lepton colliders and gravitational waves*, *Phys. Rev. D* **104** (2021) 053004 [arXiv:2012.03920] [INSPIRE].
- [69] X. Deng, X. Liu, J. Yang, R. Zhou and L. Bian, *Heavy dark matter and Gravitational waves*, *Phys. Rev. D* **103** (2021) 055013 [arXiv:2012.15174] [INSPIRE].
- [70] W. Chao, X.-F. Li and L. Wang, *Filtered pseudo-scalar dark matter and gravitational waves from first order phase transition*, *JCAP* **06** (2021) 038 [arXiv:2012.15113] [INSPIRE].
- [71] Z. Zhang, C. Cai, X.-M. Jiang, Y.-L. Tang, Z.-H. Yu and H.-H. Zhang, *Phase transition gravitational waves from pseudo-Nambu-Goldstone dark matter and two Higgs doublets*, *JHEP* **05** (2021) 160 [arXiv:2102.01588] [INSPIRE].
- [72] J. Liu, X.-P. Wang and K.-P. Xie, *Searching for lepton portal dark matter with colliders and gravitational waves*, *JHEP* **06** (2021) 149 [arXiv:2104.06421] [INSPIRE].
- [73] E. Witten, *Cosmological Consequences of a Light Higgs Boson*, *Nucl. Phys. B* **177** (1981) 477 [INSPIRE].
- [74] A. H. Guth and E. J. Weinberg, *Cosmological Consequences of a First Order Phase Transition in the SU(5) Grand Unified Model*, *Phys. Rev. D* **23** (1981) 876 [INSPIRE].
- [75] P. J. Steinhardt, *The Weinberg-Salam Model and Early Cosmology*, *Nucl. Phys. B* **179** (1981) 492 [INSPIRE].
- [76] P. J. Steinhardt, *Relativistic Detonation Waves and Bubble Growth in False Vacuum Decay*, *Phys. Rev. D* **25** (1982) 2074 [INSPIRE].
- [77] E. Witten, *Cosmic Separation of Phases*, *Phys. Rev. D* **30** (1984) 272 [INSPIRE].
- [78] M. E. Shaposhnikov, *Baryon Asymmetry of the Universe in Standard Electroweak Theory*, *Nucl. Phys. B* **287** (1987) 757 [INSPIRE].
- [79] LIGO SCIENTIFIC, VIRGO collaboration, *Observation of Gravitational Waves from a Binary Black Hole Merger*, *Phys. Rev. Lett.* **116** (2016) 061102 [arXiv:1602.03837] [INSPIRE].
- [80] C. Caprini et al., *Detecting gravitational waves from cosmological phase transitions with LISA: an update*, *JCAP* **03** (2020) 024 [arXiv:1910.13125] [INSPIRE].
- [81] LISA collaboration, *Laser Interferometer Space Antenna*, arXiv:1702.00786 [INSPIRE].
- [82] J. Crowder and N. J. Cornish, *Beyond LISA: Exploring future gravitational wave missions*, *Phys. Rev. D* **72** (2005) 083005 [gr-qc/0506015] [INSPIRE].

- [83] W. A. Bardeen, *On naturalness in the standard model*, in *Ontake Summer Institute on Particle Physics Ontake Mountain, Japan, August 27-September 2, 1995*, 1995 [INSPIRE].
- [84] S. R. Coleman and E. J. Weinberg, *Radiative Corrections as the Origin of Spontaneous Symmetry Breaking*, *Phys. Rev. D* **7** (1973) 1888 [INSPIRE].
- [85] PLANCK collaboration, *Planck 2018 results. VI. Cosmological parameters*, *Astron. Astrophys.* **641** (2020) A6 [arXiv:1807.06209] [INSPIRE].
- [86] LUX collaboration, *Results from a search for dark matter in the complete LUX exposure*, *Phys. Rev. Lett.* **118** (2017) 021303 [arXiv:1608.07648] [INSPIRE].
- [87] PANDAX-II collaboration, *Dark Matter Results from First 98.7 Days of Data from the PandaX-II Experiment*, *Phys. Rev. Lett.* **117** (2016) 121303 [arXiv:1607.07400] [INSPIRE].
- [88] XENON collaboration, *Dark Matter Search Results from a One Ton-Year Exposure of XENON1T*, *Phys. Rev. Lett.* **121** (2018) 111302 [arXiv:1805.12562] [INSPIRE].
- [89] J. Billard, L. Strigari and E. Figueroa-Feliciano, *Implication of neutrino backgrounds on the reach of next generation dark matter direct detection experiments*, *Phys. Rev. D* **89** (2014) 023524 [arXiv:1307.5458] [INSPIRE].
- [90] T. Hur, H.-S. Lee and S. Nasri, *A Supersymmetric $U(1)$ -prime model with multiple dark matters*, *Phys. Rev. D* **77** (2008) 015008 [arXiv:0710.2653] [INSPIRE].
- [91] ATLAS collaboration, *Observation of a new particle in the search for the Standard Model Higgs boson with the ATLAS detector at the LHC*, *Phys. Lett. B* **716** (2012) 1 [arXiv:1207.7214] [INSPIRE].
- [92] CMS collaboration, *Observation of a New Boson at a Mass of 125 GeV with the CMS Experiment at the LHC*, *Phys. Lett. B* **716** (2012) 30 [arXiv:1207.7235] [INSPIRE].
- [93] D. Barducci, G. Belanger, J. Bernon, F. Boudjema, J. Da Silva, S. Kraml et al., *Collider limits on new physics within micrOMEGAs-4.3*, *Comput. Phys. Commun.* **222** (2018) 327 [arXiv:1606.03834] [INSPIRE].
- [94] M. W. Goodman and E. Witten, *Detectability of Certain Dark Matter Candidates*, *Phys. Rev. D* **31** (1985) 3059 [INSPIRE].
- [95] S. Kanemura, S. Matsumoto, T. Nabeshima and N. Okada, *Can WIMP Dark Matter overcome the Nightmare Scenario?*, *Phys. Rev. D* **82** (2010) 055026 [arXiv:1005.5651] [INSPIRE].
- [96] DARWIN collaboration, *DARWIN: towards the ultimate dark matter detector*, *JCAP* **11** (2016) 017 [arXiv:1606.07001] [INSPIRE].
- [97] E. Gildener and S. Weinberg, *Symmetry Breaking and Scalar Bosons*, *Phys. Rev. D* **13** (1976) 3333 [INSPIRE].

- [98] Y. Tang, *Vacuum Stability in the Standard Model*, *Mod. Phys. Lett. A* **28** (2013) 1330002 [[arXiv:1301.5812](#)] [[INSPIRE](#)].
- [99] A. Karam and K. Tamvakis, *Dark matter and neutrino masses from a scale-invariant multi-Higgs portal*, *Phys. Rev. D* **92** (2015) 075010 [[arXiv:1508.03031](#)] [[INSPIRE](#)].
- [100] A. Karam and K. Tamvakis, *Dark Matter from a Classically Scale-Invariant $SU(3)_X$* , *Phys. Rev. D* **94** (2016) 055004 [[arXiv:1607.01001](#)] [[INSPIRE](#)].
- [101] L. Dolan and R. Jackiw, *Symmetry Behavior at Finite Temperature*, *Phys. Rev. D* **9** (1974) 3320 [[INSPIRE](#)].
- [102] M. E. Carrington, *The Effective potential at finite temperature in the Standard Model*, *Phys. Rev. D* **45** (1992) 2933 [[INSPIRE](#)].
- [103] D. Croon, O. Gould, P. Schicho, T. V. I. Tenkanen and G. White, *Theoretical uncertainties for cosmological first-order phase transitions*, *JHEP* **04** (2021) 055 [[arXiv:2009.10080](#)] [[INSPIRE](#)].
- [104] O. Gould and T. V. I. Tenkanen, *On the perturbative expansion at high temperature and implications for cosmological phase transitions*, *JHEP* **06** (2021) 069 [[arXiv:2104.04399](#)] [[INSPIRE](#)].
- [105] Z. Kang and J. Zhu, *Scale-genesis by Dark Matter and Its Gravitational Wave Signal*, *Phys. Rev. D* **102** (2020) 053011 [[arXiv:2003.02465](#)] [[INSPIRE](#)].
- [106] A. Masoumi, K. D. Olum and J. M. Wachter, *Approximating tunneling rates in multi-dimensional field spaces*, *JCAP* **10** (2017) 022 [[arXiv:1702.00356](#)] [[INSPIRE](#)].
- [107] D. Bodeker and G. D. Moore, *Can electroweak bubble walls run away?*, *JCAP* **05** (2009) 009 [[arXiv:0903.4099](#)] [[INSPIRE](#)].
- [108] S. J. Huber and T. Konstandin, *Gravitational Wave Production by Collisions: More Bubbles*, *JCAP* **09** (2008) 022 [[arXiv:0806.1828](#)] [[INSPIRE](#)].
- [109] H.-K. Guo, K. Sinha, D. Vagie and G. White, *Phase Transitions in an Expanding Universe: Stochastic Gravitational Waves in Standard and Non-Standard Histories*, *JCAP* **01** (2021) 001 [[arXiv:2007.08537](#)] [[INSPIRE](#)].
- [110] M. Hindmarsh, S. J. Huber, K. Rummukainen and D. J. Weir, *Numerical simulations of acoustically generated gravitational waves at a first order phase transition*, *Phys. Rev. D* **92** (2015) 123009 [[arXiv:1504.03291](#)] [[INSPIRE](#)].
- [111] C. Caprini, R. Durrer and G. Servant, *The stochastic gravitational wave background from turbulence and magnetic fields generated by a first-order phase transition*, *JCAP* **12** (2009) 024 [[arXiv:0909.0622](#)] [[INSPIRE](#)].
- [112] C. Caprini et al., *Science with the space-based interferometer eLISA. II: Gravitational waves from cosmological phase transitions*, *JCAP* **04** (2016) 001 [[arXiv:1512.06239](#)] [[INSPIRE](#)].

- [113] M. Kamionkowski, A. Kosowsky and M. S. Turner, *Gravitational radiation from first order phase transitions*, *Phys. Rev. D* **49** (1994) 2837 [[astro-ph/9310044](#)] [[INSPIRE](#)].
- [114] T. Alanne, T. Hugle, M. Platscher and K. Schmitz, *A fresh look at the gravitational-wave signal from cosmological phase transitions*, *JHEP* **03** (2020) 004 [[arXiv:1909.11356](#)] [[INSPIRE](#)].
- [115] K. Schmitz, *New Sensitivity Curves for Gravitational-Wave Signals from Cosmological Phase Transitions*, *JHEP* **01** (2021) 097 [[arXiv:2002.04615](#)] [[INSPIRE](#)].
- [116] K. Schmitz, *LISA Sensitivity to Gravitational Waves from Sound Waves*, *Symmetry* **12** (2020) 1477 [[arXiv:2005.10789](#)] [[INSPIRE](#)].
- [117] T. Cohen, D. E. Morrissey and A. Pierce, *Changes in Dark Matter Properties After Freeze-Out*, *Phys. Rev. D* **78** (2008) 111701 [[arXiv:0808.3994](#)] [[INSPIRE](#)].